Acta Cryst A FOUNDATIONS ADVANCES
ISSN 2053-2733

Spin-resolved atomic orbital model refinement for combined charge and spin density analysis: application to the $YTiO_3$ perovskite

Iurii Kibalin,[a,b,c] Ariste Bolivard Voufack,[b,d] Mohamed Souhassou,[b]* Béatrice Gillon,[a] Jean-Michel Gillet,[e] Nicolas Claiser,[b] Arsen Gukasov,[a] Florence Porcher[a] and Claude Lecomte[b]

[a]Laboratoire Léon Brillouin, CEA-CNRS, CE-Saclay, Gif-sur-Yvette, 91191, France, [b]CRM2, Institut Jean Barriol, Lorraine University and CNRS, BP239, Vandoeuvre-les-Nancy, F54506, France, [c]PNPI, NRC 'Kurchatov Institute', Orlovarosha, Gatchina, Leningrad region 188300, Russian Federation, [d]MACETS, Faculté des Sciences, Université de Dschang, BP 67, Dschang, Cameroon, and [e]Laboratoire SPMS, UMR 8580, CentraleSupélec, Paris-Saclay University, Gif-sur-Yvette, 91191, France. *Correspondence e-mail: mohamed.souhassou@univ-lorraine.fr

Received 3 July 2020
Accepted 17 December 2020

Edited by P. M. Dominiak, University of Warsaw, Poland

Keywords: atomic orbital model; two-center term; polarized neutron diffraction; X-ray diffraction; perovskite; spin density; charge density.

Supporting information: this article has supporting information at journals.iucr.org/a

A new crystallographic method is proposed in order to refine a spin-resolved atomic orbital model against X-ray and polarized neutron diffraction data. This atomic orbital model is applied to the $YTiO_3$ perovskite crystal, where orbital ordering has previously been observed by several techniques: X-ray diffraction, polarized neutron diffraction and nuclear magnetic resonance. This method gives the radial extension, orientation and population of outer atomic orbitals for each atom. The interaction term between Ti^{3+}, Y^{3+} cations and O^{2-} ligands has been estimated. The refinement statistics obtained by means of the orbital method are compared with those obtained by the multipole model previously published.

1. Introduction

The representation of experimentally derived electron density plays an important role in the characterization of chemical interactions; this density may be described by a set of model parameters or by numerical values on a 3D grid. The former is the most suitable for electrostatic calculations and topological analysis since all properties can be calculated analytically.

The multipole model was developed and widely used for the analysis of charge density distribution measured by X-ray diffraction (XRD) (Bentley & Stewart, 1973; Stewart, 1969; Hansen & Coppens, 1978). It was later extended to spin density (Brown *et al.*, 1979). In this case, electron density is expressed as a linear combination of spherical harmonics. Such a model has been remarkably successful in estimating various electrostatic physical quantities such as electrostatic fields, electrostatic potentials and electrostatic moments (Jelsch *et al.*, 2005). When the system possesses magnetic properties, knowledge of the electron spin density distribution is needed. The polarized neutron diffraction (PND) method provides the spin distribution at the atomic scale. A spin-resolved multipole model combining information from XRD and PND experiments was developed in our laboratories and implemented in the *MOLLYNX* program (Deutsch *et al.*, 2012). It has been successfully applied to organic radicals (Voufack *et al.*, 2017), coordination compounds (Deutsch *et al.*, 2014) and inorganic perovskites (Voufack *et al.*, 2019).

However, the multipole model is not suitable for retrieving some fundamental quantities such as first-order density

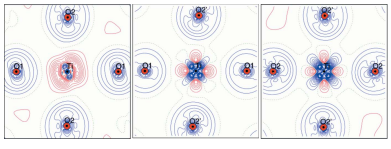

© 2021 International Union of Crystallography

matrices or the orbital representation of wavefunctions. Nevertheless, the multipole model deduced from charge density analysis does not provide the populations of atomic orbitals; they are approximately estimated by the Stevens method (Stevens, 1980) extended by Holladay and Coppens (Holladay *et al.*, 1983). It should be noted that an atomic orbital model refinement was previously developed for spin density analysis only. In this model the atomic wavefunction is constructed as a linear combination of the atomic orbitals localized on each atom which are supposed to carry unpaired electrons, the populations of which are refined on the basis of the PND data (Schweizer & Ressouche, 2001).

The present model is based on quantum-mechanical orbitals, also proposed by K. Tanaka for charge density analysis, and provides the aforementioned physical quantities (Tanaka, 1988). Tanaka's model gives access to molecular or atomic orbitals from the structure factors measured by XRD. Nevertheless, the difficulty in implementing this model lies in the refinement of orthogonal wavefunctions ψ_i defined for each electron in the system. Because the constraint conditions on the parameters of wavefunctions increase quadratically with the number of electrons, the least-squares refinement usually failed for a large number of non-linear constraints. The problem was circumvented by neglecting overlap between atomic orbitals located on different atoms (Tanaka *et al.*, 2008), but it does not allow a fully quantitative description of the inter-atomic interactions. Figgis and coworkers have also proposed such a model applied for example to a copper complex (Bytheway *et al.*, 2001).

The objective of the paper is to describe a spin-resolved simplified atomic orbital model where interaction between atoms is accounted for. The model was implemented in our previously developed program *MOLLYNX* for joint XRD and PND refinement (Deutsch *et al.*, 2012). The following sections are considered in the paper: description of the atomic orbital model, calculation of the electron density, XRD and PND structure factors, and refinement using non-linear least-squares refinement constraints. Then the validity of this spin-resolved atomic orbital model is demonstrated using $YTiO_3$ perovskite XRD and PND data. The refinement quality is compared with that obtained with the spin-resolved multipolar model (Vouffack *et al.*, 2019). The contribution of the different atomic orbitals to the magnetization of the sample is discussed.

2. Atomic orbital model

2.1. Total electron density

In this model, the total electron density $\rho(\mathbf{r})$ is represented as a sum of two terms: the density of electrons centered on atoms and that lying on the bonds $\rho_b(\mathbf{r})$. The first contribution is itself a sum of spherical 'core' $\rho_c(\mathbf{r})$ and non-spherical external 'valence' terms $\rho_v(\mathbf{r})$:

$$\rho(\mathbf{r}) = \rho_c(\mathbf{r}) + \rho_v(\mathbf{r}) + \rho_b(\mathbf{r}). \quad (1)$$

To construct 'core' terms the radial function $R_i(r)$ for each shell has to be defined with electron populations p_i on the shell i for all A atoms:

$$\rho_c(\mathbf{r}) = \sum_A \sum_i \frac{1}{4\pi} p_i R_i^2(|\mathbf{r} - \mathbf{r}_A|). \quad (2)$$

The radial functions (R_i) implemented in the *MOLLYNX* program (Deutsch *et al.*, 2012) are described in the following subsection. The populations p_i are, respectively, equal to 2, 6 and 10 for s, p and d full core shells.

The 'valence' term can be represented through atomic orbitals ϕ_i, which are linear combinations, with c_{iv} coefficients, of orthonormal basis functions χ_v:

$$\phi_i = \sum_v c_{iv}\chi_v.$$

Although the orbitals $\{\phi_i\}$ can be defined arbitrarily, orthonormal atomic orbitals are used to reduce the multiplicity in representation of density $\rho_v(\mathbf{r})$.

The density $\rho_v(\mathbf{r})$ is the sum over all the squared modulus of valence orbitals ϕ_i having population n_i:

$$\rho_v(\mathbf{r}) = \sum_A \sum_i n_i \sum_{\mu,\nu} c_{i\mu}c_{iv}\chi_\mu(\mathbf{r} - \mathbf{r}_A)\chi_v(\mathbf{r} - \mathbf{r}_A). \quad (3)$$

Here A runs over the number of atoms, i over the number of valence atomic orbitals and μ, ν run over basis functions $\{\chi_\mu\}$.

To describe the total electron density, the density $\rho_b(\mathbf{r})$ of bonded pairs of atomic orbitals ϕ_i and ϕ_j centered on different interacting atoms A and B is used (two-center orbital product):

$$\rho_b(\mathbf{r}) = \sum_{A\neq B} \sum_{i,j} \frac{n_{ij}}{N_{ij}} \sum_{\mu,\nu} c_{i\mu}c_{j\nu}\chi_\mu(\mathbf{r} - \mathbf{r}_A)\chi_v(\mathbf{r} - \mathbf{r}_B). \quad (4)$$

The parameter n_{ij} characterizes the electron population of the orbital product $\phi_i\phi_j$. The normalization constant N_{ij} is the orbital overlap: $N_{ij} = \int \phi_i(\mathbf{r} - \mathbf{r}_A)\phi_j(\mathbf{r} - \mathbf{r}_B)\,\mathrm{d}^3\mathbf{r}$. Zero constant N_{ij} corresponds to orthogonal orbitals, for which the orbital product cannot be populated. This term is supposed to be large for covalent bonds.

2.2. Basis functions

For hydrogen-like orbitals (s, p, d and so on), the orbital basis functions may be expressed as the product of radial $R_\mu(r)$ and real spherical harmonics $Y_{lm}(\theta, \phi)$ functions:

$$\chi_\mu(r, \theta, \phi) = R_\mu(r)Y_{lm}(\theta, \phi). \quad (5)$$

Several functions have been proposed to describe the radial function (Stewart, 1969; Bonham, 1965; Stewart *et al.*, 1965). Here we use the following description: according to Clementi & Roetti (1974) the radial function for orbitals of isolated atoms can be expressed as a sum of Slater functions (Slater-type orbital, STO):

$$R_\mu(r) = \sum_{k=1}^{N_{STO}} p_k \frac{(2\zeta_k)^{n_k+1/2}}{(2n_k!)^{1/2}} r^{n_k-1}\exp(-\zeta_k r). \quad (6)$$

The expansion of the radial part on Gaussian functions is widely used in *ab initio* calculations and the radial function can

also be described via Gaussian-type orbitals (GTOs). The analytical expression is

$$R_\mu(r) = \frac{2^{n+3/4} r^{n-1}}{\pi^{1/4}[(2n-1)!!]^{1/2}} \sum_{k=1}^{N_{\rm GTO}} p_k \alpha_k^{(2n+1)/4} \exp(-\alpha_k r^2). \quad (7)$$

GTOs have proved to be more convenient for computing two-center integrals than STOs and have thus become more popular for many numerical applications.

The parameters p_k, ζ_k, α_k are tabulated values which can be found in handbooks (Clementi & Roetti, 1974; Schuchardt *et al.*, 2007) for both models for each neutral atom shell.

The extension of atomic orbitals depends on the nature of chemical bonding between neighboring atoms. The radial function can be modified by means of the expansion contraction coefficient κ (also called the scaling parameter) which is a multiplying factor of the radius r.

2.3. Spin and charge structure factors

The interpretation of XRD and PND experiments requires an accurate estimation of electronic and magnetic structure factors, which are Fourier transforms of the charge and spin densities, respectively. As the Fourier transform is a linear operation, structure factors can also be separated into 'core' $F_{\rm c}(\mathbf{H})$, 'valence' $F_{\rm v}(\mathbf{H})$ and 'bond' terms $F_{\rm b}(\mathbf{H})$.

The Fourier transform of the 'core' electron density is expressed as

$$F_{\rm c}(\mathbf{H}) = \sum_A T_A \left[\sum_i \frac{p_i}{4\pi} \int_0^\infty R_i^2(r) j_0(2\pi H r)\, {\rm d}r + F_A \right], \quad (8)$$

where $j_0(2\pi Hr)$ is a zeroth-order spherical Bessel function. T_A is the Debye–Waller factor of atom A (Shmueli, 2001). The complex value F_A is the anomalous scattering part of atom A in the case of X-rays only. The integral in (8) has an analytical solution when the radial function R_μ is expressed through STOs (Avery & Watson, 1977) or GTOs (Chandler & Spackman, 1978).

The 'valence' component of the structure factor includes the contribution from the outer orbitals located on the same atom:

$$F_{\rm v}(\mathbf{H}) = \sum_A T_A \sum_i n_i \sum_{\mu,\nu} c_{i\mu} c_{i\nu} \int \chi_\mu \chi_\nu \exp(i2\pi \mathbf{H}\cdot\mathbf{r})\, {\rm d}^3\mathbf{r}. \quad (9)$$

The integral $\int \chi_\mu \chi_\nu \exp(i2\pi \mathbf{H}\cdot\mathbf{r})\, {\rm d}^3\mathbf{r}$ has a simple analytical solution for STOs and GTOs (Stewart, 1969; Tanaka, 1988; Chandler & Spackman, 1978; Shmueli, 2001; Tanaka *et al.*, 2008). Note that the one-center orbital product can be represented as a radial function multiplied by a sum over spherical harmonic functions weighted by Clebsch–Gordan coefficients. It follows that the modeled density is formally equivalent to the multipole model description extended up to fourth-order spherical functions for the valence shell p, and up to sixth-order spherical functions for the valence shell d.

The 'bond' term describes electrons shared by two neighboring atoms. Therefore, the Fourier transforms of two-center orbital products have to be calculated. If the radial function is expressed through GTOs, the Fourier transform has an analytical expression (Avery & Watson, 1977). Therefore, as the integral solution for STOs is expressed through generalized hypergeometric functions (Niehaus *et al.*, 2008; Vuković & Dmitrović, 2010), in the present work the 'bond' structure factor is calculated using GTOs which are easier to handle than STOs.

Nevertheless, STOs are better suited than GTOs to represent electron wavefunctions. The expansion over STOs is therefore used for the structure factor calculations of 'core' and 'valence' terms, while GTOs are applied only for the 'bond' term calculations.

XRD allows reconstruction of the total electron distribution, while PND provides information about the spin density, *i.e.* the unpaired electron distribution. These two quantities can be expressed in terms of spin-resolved populations of atomic orbitals representing, respectively, the sum and the difference between spin-up $n_i^\uparrow$, $n_{ij}^\uparrow$ and spin-down $n_i^\downarrow$, $n_{ij}^\downarrow$ populations. The charge and spin structure factors are thus calculated as

$$F_{\rm charge} = F_{\rm c} + F_{\rm v}^\uparrow + F_{\rm v}^\downarrow + F_{\rm b}^\uparrow + F_{\rm b}^\downarrow, \quad (10)$$

$$F_{\rm spin} = F_{\rm v}^\uparrow - F_{\rm v}^\downarrow + F_{\rm b}^\uparrow - F_{\rm b}^\downarrow, \quad (11)$$

where each spin-dependent component is calculated using the corresponding spin-dependent populations n_i and n_{ij}.

The relations between the corresponding structure factors and the diffraction intensities (in the case of XRD) or flipping ratios (in the case of PND) can be found in the literature (Stewart *et al.*, 1965; Gillon & Becker, 2011).

2.4. Constraints over model parameters

The described model is fitted against the XRD and PND data by a least-squares refinement procedure. As usual, several constraints must be applied to the refined parameters.

To ensure the electroneutrality of the unit cell, the total number of electrons is required to remain unchanged in the unit cell:

$$\sum_A \sum_i \left(n_i^\uparrow + n_i^\downarrow\right) + \sum_{A>B} \sum_{i,j} \left(n_{ij}^\uparrow + n_{ij}^\downarrow\right) = {\rm const}. \quad (12)$$

A similar constraint concerns the conservation of the magnetic moment, *i.e.* the number of unpaired electrons in the unit cell. It is written as

$$\sum_A \sum_i \left(n_i^\uparrow - n_i^\downarrow\right) + \sum_{A>B} \sum_{i,j} \left(n_{ij}^\uparrow - n_{ij}^\downarrow\right) = {\rm const}. \quad (13)$$

The refinement of the orthonormal atomic orbitals $\{\phi_i\}$ leads to additional constraints on the orientation parameters $\{c_{i\mu}\}$:

$$\sum_\mu c_{i\mu} c_{j\mu} = \delta_{ij}, \quad (14)$$

for each pair of orbitals ϕ_i and ϕ_j located on the same atom. δ_{ij} is the Kronecker delta piecewise function. The cross-term $c_{i\mu}c_{j\nu}$ is absent in (14) due to the mutual orthogonality of the orbital basis functions χ_μ and χ_ν.

The electroneutrality and spin constraints are of linear type. There are several methods devoted to the implementation of such constraints in the least-squares refinement procedure (Raymond, 1972; Hamilton, 1964). One of the usual methods in crystallography is the Hamilton method (Hamilton, 1964). In order to introduce non-linear constraints (orthonormal atomic orbitals $\{\phi_i\}$) the classical Hamilton method has been extended. The mathematical description is given in Appendix *A*.

3. Spin-resolved electron density in $YTiO_3$

The performance and validity of this new method are evaluated on the $YTiO_3$ perovskite crystal; its charge and spin densities are decomposed into 'core', 'valence' and 'bond' contributions. Fig. 1 shows the structure of $YTiO_3$ (orthorhombic, space group *Pnma*). The Ti^{3+} ion sits on the center of a centrosymmetric distorted oxygen octahedron. The Y^{3+} ion sits on a mirror plane and is coordinated by eight oxygen atoms forming a distorted square antiprism.

This perovskite has been studied intensively by means of various experimental and theoretical methods such as nuclear magnetic resonance (Itoh & Tsuchiya, 2001), polarized (Akimitsu *et al.*, 2001) and unpolarized (Ulrich *et al.*, 2002) neutron diffraction, inelastic neutron scattering (Li *et al.*, 2014), resonant X-ray scattering (Nakao *et al.*, 2002), soft X-ray linear dichroism (Iga *et al.*, 2004), X-ray magnetic diffraction (XMD) (Ito *et al.*, 2004), Compton scattering (Tsuji *et al.*, 2008) and elastic X-ray scattering (Hester *et al.*, 1997). Such interest is mainly due to the existence of an antiferromagnetic orbital ordering in the ferromagnetic state of $YTiO_3$ (its Curie temperature is 30 K). Theoretical studies using unrestricted Hartree–Fock calculations and density functional theory with generalized gradient approximation predicted the wavefunction of the 3*d* electrons of titanium atoms to be a linear combination of $|xz\rangle$ and $|yz\rangle$ orbitals in the t_{2g} state (Mochizuki & Imada, 2004). The experimental estimation of the atomic orbitals orientation from PND and XMD data (Akimitsu *et al.*, 2001; Ito *et al.*, 2004; Kibalin *et al.*, 2017) was performed within the approximation of a single unpaired electron located on the $|3d\rangle$ orbitals of the octahedrally coordinated titanium atom. The results are in good agreement with the theoretical predictions (Kibalin *et al.*, 2017).

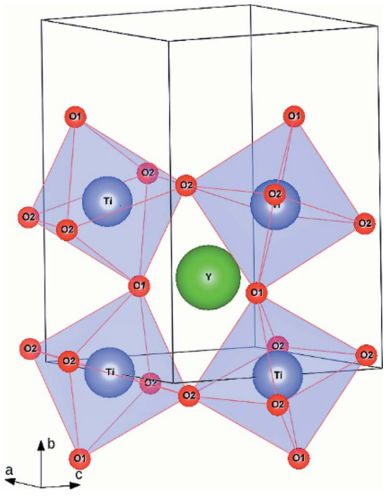

Figure 1
Crystal structure of $YTiO_3$ (orthorhombic, space group *Pnma*).

In this paper we investigate beyond the limitation of one unpaired electron and take advantage of the spin-resolved atomic orbital model explained above to perform a combined analysis of charge and spin densities.

3.1. Experiments

The charge density analysis was made using synchrotron diffraction data (SPRING8 beamline BL02B2) on a single crystal (0.021 × 0.100 × 0.109 mm) at 20 K in the ferromagnetic phase. A short wavelength (0.353 Å) was used to reduce absorption and extinction effects. The details of the experimental conditions are given in our previous paper (Voufack *et al.*, 2019).

The PND measurements were performed on the thermal polarized neutron lifting-counter diffractometer 6T2 and the hot polarized neutron two-axis diffractometer 5C1 (LLB-Orphée, Saclay). The data were obtained at 5 K, in the ferromagnetic phase, under an applied magnetic field of 5 T, parallel to the *a*, *b* and *c* axes of the single-crystalline sample, with two neutron wavelengths, 1.4 Å (6T2 diffractometer) and 0.84 Å (5C1 diffractometer). The incomplete beam polarization and extinction effects were corrected for. The details of the neutron measurements are provided in the work of Kibalin *et al.* (2017).

3.2. Model parameters

To specify the orbital model, 'core', 'valence' and 'bond' terms have to be defined. The parameters characterizing the 'core' term are not refined, in contrast to the other two terms.

The populations of the 'core' shells p_i in equation (8) have been taken as in [Kr], [Ar] and [He] for yttrium, titanium and oxygen atoms, respectively. The radial function is expanded over Slater functions for each shell. The radial function parameters p_k, ζ_k can be found in the work of Clementi & Roetti (1974).

The 'valence' orbitals have been chosen for each atom as 4*d*, 5*s* for yttrium, 3*d*, 4*s* for titanium and 2*s*, 2*p* for oxygen using Slater-type radial functions of 'valence' orbitals (Clementi & Roetti, 1974). The refined parameters are: the linear combination coefficients ($c_{i\mu}$), the spin-dependent partial orbital populations ($n_i^{\uparrow}$, $n_i^{\downarrow}$) and the expansion contraction coefficient (κ), which modulates the radial function of valence orbital shells [in equations (6) and (7)].

The refinement was first carried out without the 'bond' term. The 'bond' terms which account for titanium–oxygen and yttrium–oxygen couplings were modeled in a second stage; O–O couplings were neglected. As explained above, GTO expansions were used to describe the radial functions only for this bond contribution. The expansion parameters are defined as the best approximation of the corresponding radial

function of 'valence' orbitals. The comparison of the radial functions for 'valence' orbitals and the 'bond' term is shown in Fig. S1 in the supporting information, together with the expansion parameters (Tables S1–S3).

No extinction effects were detected on the low-order reflections. The positions of atoms and their harmonic Debye–Waller factors were simultaneously refined for XRD and PND data using the UNIT weighting scheme. For a discussion on the weighting scheme see the work of Deutsch *et al.* (2012). For X-ray data, anharmonicity effects have been taken into account (Gram–Charlier expansion) as in our previous work (Voufack *et al.*, 2019).

3.3. Agreement factors

The experimental data were described in the framework of two different atomic orbital models, including or excluding the 'bond' term. In order to assess the quality of the refinements a comparison with the widely used multipole model is given. The statistical agreement factors for multipole and orbital models are provided in Table 1. The agreement factors and goodness-of-fit for all models have similar values. In all cases, the agreement factors $R_w(|F_{\rm charge}|)$ for XRD data are lower than 1.5%, showing a very reliable description of electron density. The agreement factors for PND data are higher, which is typical for spin density analysis where weighted agreement factors $R_w(|R-1|)$ usually amount to 10%.

The X-ray goodness-of-fits for reflections grouped in the 0.1 Å^{-1} range of $\sin\theta/\lambda$ clearly show only very tiny differences in data description by the multipole and orbital models (Fig. 2). The orbital model yields larger values of $\chi^2_{\rm XRD}$ and $\chi^2_{\rm PND}$ than the multipole model, as the latter has higher flexibility (*i.e* a higher number of parameters are refined). The distribution of reflections over $\sin\theta/\lambda$ is shown on the same figure by a histogram. Small discrepancies between the two models lie in the $\sin\theta/\lambda$ range [0.2−0.35 Å^{-1}] as it corresponds to the largest d electron scattering (see Fig. 3). The description of the high-order experimental X-ray data ($\sin\theta/\lambda > 0.8$ Å^{-1}) is independent of the model used. The refinement of atomic positions and Debye–Waller factors has the strongest influence on the intensity of high-order reflections, which are found to be similar for the multipole and orbital models (Tables S4–S6 in the supporting information). In conclusion, on the sole basis of least-squares statistical indices, it is not possible to decide which model is the best. The orbital model describes experimental data with a smaller number of physically meaningful parameters than the multipole model and therefore is better than the latter.

The introduction of 'bond' terms only slightly improves the description of the low-order reflections (see Fig. S3). The small contribution of the 'bond' terms is related to the small covalent contribution between the Ti and O atoms. We expect the impact of 'bond' terms to be more visible for a crystal like pyrite or a molecular crystal where covalency is the leading

Table 1
Statistical agreement factors for joint refinement procedure of XRD and PND data in the framework of the multipole model, and the atomic orbital model without the 'bond' term (orbital I) and with the 'bond' term (orbital II).

The statistics of spherical atom refinement are given for comparison. Agreement factors are calculated on $|F_{\rm charge}|$ and $|R-1|$ for XRD and PND data, respectively.

Parameter	Multipole	Orbital I	Orbital II	Spherical	Data
R (%)	1.40	1.39	1.39	1.47	XRD
wR (%)	1.12	1.12	1.11	1.27	N_{hkl} = 4521
$(\chi^2/N_{hkl})^{1/2}$	1.18	1.18	1.18	1.34	
R (%)	17.21	19.47	19.47	57.83	PND
wR (%)	8.84	9.21	9.20	29.55	N_{hkl} = 291
$(\chi^2/N_{hkl})^{1/2}$	4.14	4.31	4.31	13.8	

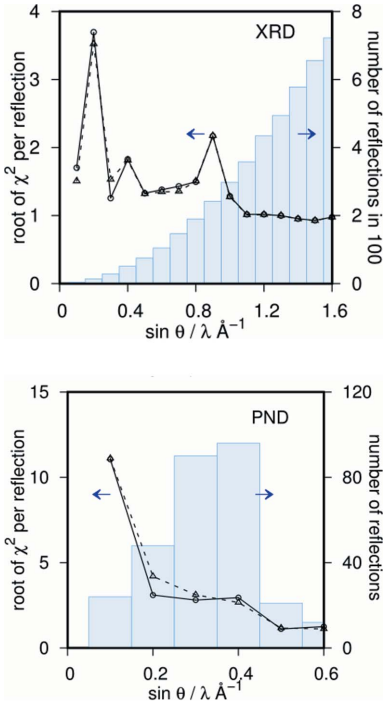

Figure 2
The goodness-of-fit of reflections grouped in 0.1 Å^{-1} ranges of $\sin\theta/\lambda$ (XRD and PND) for multipole (circles with solid line) and orbital models without the 'bond' term (triangles with a dotted line). The histogram shows a distribution of reflections (in hundreds for XRD) over $\sin\theta/\lambda$.

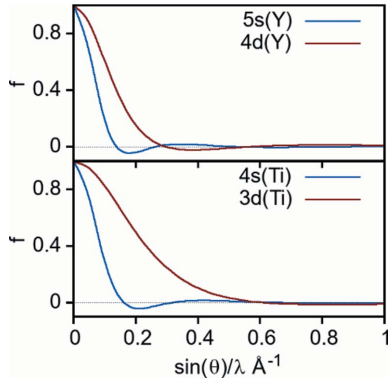

Figure 3
Normalized valence scattering factors 5*s* and 4*d* of Y (top) and 4*s* and 3*d* of Ti (bottom).

term. In the present paper we thus decided to discuss the atomic orbital model where the 'bond' term is excluded (model I).

Model I, model II and the multipolar model give similar residual densities. In all cases, the largest residual charge densities are observed around the titanium and yttrium atoms. Most undescribed residual density is directed along the [100] direction (dotted lines on Fig. 4). We suppose that this noise is due to insufficient absorption corrections for XRD data. It is a common problem when the studied sample has a complex shape. Also, the XRD data were not corrected for multiple scattering, and this phenomenon increases with the number of electrons. Therefore any uncertainty in estimations increases the residual density around the most significant scatterers along the same direction.

The residual charge density has a random distribution in the other planes (see Fig. S4) proving that the atomic orbital model correctly describes the experimental data. Note that the residual density is larger in the Y—O1—O1 plane as it is a mirror plane.

3.4. Spin-resolved electron density analysis

XRD is highly sensitive to the radial distribution of atomic orbitals. It allows an estimation of their size via the expansion contraction coefficient. The κ parameters of Y and Ti atoms 'valence' orbitals (4*d* for yttrium and 4*s*, 3*d* for titanium) are far from unity (see Table 2). This corresponds to the shrinking of outer electronic orbitals, as yttrium and titanium are giving away their electrons to oxygen atoms. Opposite changes are found for oxygen atoms where the *p*-shell κ parameter is less than one. Thus, the O electronic orbitals are more diffuse compared with the neutral atom as oxygen accepts additional electrons coming from titanium and yttrium.

The 'valence' charge and spin populations of all atoms are summarized in Table 2 together with the expansion coefficients κ of the 'valence' orbitals. The formal number of electrons on the 'valence' orbitals for neutral and fully ionized atoms is also reported. Clearly the estimated net atomic charges have intermediate values between neutral and fully ionized states, which is a typical situation in charge density analysis. However, the Ti and O net charges obtained by the wavefunction model I differ greatly from those obtained using the multipole model: the titanium is more positively charged (1.5+), giving more electrons to the O1 and O2 atoms (1.0−) in model I. This is in line with the expansion contraction coefficients as the wavefunction models give larger κ than the multipole ones (Table 2). It can be noted that the charges obtained from model I (and model II) are very close to those calculated by integration over Bader atomic basins (Bader, 1990) (respectively, +1.47 and −1.05); this is probably due to the small contribution of covalency in this perovskite.

The total magnetization per titanium atom is 0.90 (1) μ_B. The unpaired electron is mostly localized on the titanium atom. The obtained magnetic moments are in line with those calculated from the multipole model. Small magnetic moments previously observed on Y and O1 (Voufack *et al.*, 2019; Kibalin *et al.*, 2017) are of the order of 1σ in the present study. In this model the estimated error bars are significantly larger than the parameter value for Y and O1. This is a consequence of the contribution of errors from both XRD and PND experiments but also of the large correlation between the

Table 2
Valence and spin populations of the 'valence' term.

κ_1 and κ_2 are the radial expansion contraction factors for 5*s*, 4*s*, 2*s* and 4*d*, 3*d*, 2*p* shells of Y, Ti, O, respectively. When no error bar is given, the parameter was fixed during the refinement procedure. These values are compared with those obtained from the joint refinement multipole model (*) and Bader integration (Voufack *et al.*, 2019) (**).

Atom	P_{val}	Net charge	Spin	κ_1	κ_2
Y	1.4 (5)	1.6 (5)	0.0 (5)	1.0	1.54 (2)
Y*	1.53 (7)	1.47 (7)	−0.03 (7)	1.03 (8)	1.49 (6)
Y**		1.80	0.066		
Ti	2.47 (8)	1.53 (8)	1.05 (8)	1.535 (4)	1.196 (2)
Ti*	3.40 (6)	0.60 (6)	1.04 (6)	1.14 (2)	0.90 (3)
Ti**		1.47	0.628		
O1	6.95 (9)	−0.95 (9)	0.00 (9)	1.0	0.934 (1)
O1*	6.66 (3)	−0.66 (3)	0.02 (3)	0.964 (4)	0.88 (7)
O1**		−1.06	0.112		
O2	7.07 (7)	−1.07 (7)	−0.05 (7)	1.0	0.921 (1)
O2*	6.70 (2)	−0.70 (2)	0.00 (2)	0.968 (2)	0.98 (7)
O2**		−1.05	0.097		

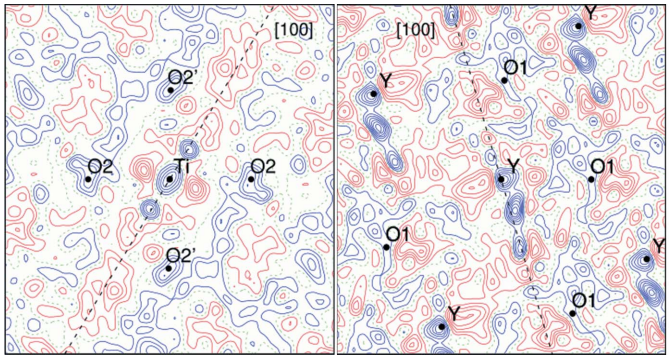

Figure 4
Residual charge density around titanium and yttrium atoms. Contours are 0.10 e Å^{-3}. Green dotted contours are zero level, red ones are negative, blue ones are positive. The [100] direction is shown by black dotted lines; 4521 reflections up to $\sin(\theta)/\lambda < 1.2$ Å^{-1}.

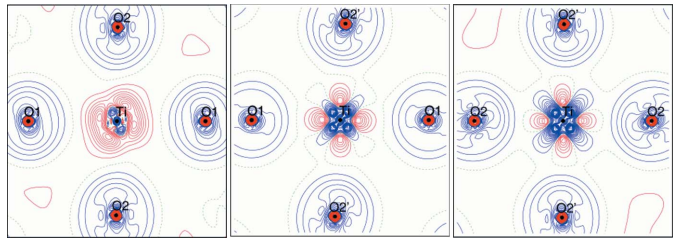

Figure 5
Static charge deformation density (model I) around the titanium atom in the *xy*, *xz* and *yz* planes of the Ti octahedron. Contour levels are 0.05 e Å^{-3}. Green dotted contours are zero level, red ones are negative, blue ones are positive

Table 3
Linear combination coefficients of the basis functions and populations of 'valence' atomic orbitals of the titanium atom.

	ϕ_1	ϕ_2	ϕ_3	ϕ_4	ϕ_5	ϕ_6
$\|4s\rangle$	1	0	0	0	0	0
$\|3d_{z^2}\rangle$	0	−0.03 (1)	−0.2 (1)	−0.5 (2)	0.22 (8)	−0.8 (2)
$\|3d_{zx}\rangle$	0	0.62 (1)	−0.2 (3)	−0.34 (5)	−0.67 (8)	0.1 (1)
$\|3d_{yz}\rangle$	0	0.78 (1)	0.3 (3)	0.19 (6)	0.53 (9)	−0.07 (9)
$\|3d_{x^2y^2}\rangle$	0	0.02 (1)	−0.5 (2)	−0.5 (1)	0.5 (2)	0.5 (2)
$\|3d_{xy}\rangle$	0	−0.09 (1)	0.76 (3)	−0.63 (4)	0.0 (3)	0.1 (2)
$n_i^{\uparrow}$	0.60 (5)	0.83 (1)	0.02 (1)	0.18 (1)	0.01 (1)	0.12 (1)
$n_i^{\downarrow}$	0.14 (5)	−0.01 (1)	0.16 (1)	0.11 (1)	0.22 (1)	0.09 (1)

parameters of atomic orbitals used for the charge and spin density analysis.

The redistribution of electrons in comparison with non-interacting neutral independent atom model (IAM) atoms is shown on the static charge deformation density (Fig. 5). The negative difference density around titanium is directed towards the positive distribution around the oxygen atoms: the depopulation of titanium e_g orbitals faces the oxygen p-filled orbitals. Titanium t_{2g} orbitals are more populated than those of the isolated neutral atom (blue contours around titanium in Fig. 5). These maps agree with the multipolar ones and with the dynamic deformation density (example in Fig. S5).

The orientations and populations of atomic orbitals of titanium are given in Table 3. A first remark is that the standard deviations obtained on the wavefunction coefficients are large for ϕ_3 ϕ_4, ϕ_5 and ϕ_6 as very few refined coefficients are statistically non-zero.

The spin density distribution of the titanium, $n_i^{\uparrow}$ and $n_i^{\downarrow}$, shows that the spin-up contribution mostly originates from the electrons located on two atomic orbitals ϕ_1 and ϕ_2 while the spin-down electrons arise from ϕ_5 and ϕ_3 (mostly $|xy\rangle$). The resulting magnetic moment is due to the $|4s\rangle$ orbital and to the linear combinations of $|zx\rangle$ and $|yz\rangle$ basis orbitals. The orientation coefficients of orbital ϕ_2 are not surprising and are in line with the work of Akimitsu *et al.* (2001). The large $|4s\rangle$ orbital population agrees with our previous work as the multipole model refinement also showed a high spherical contribution to the magnetic moment localized on the titanium atom.

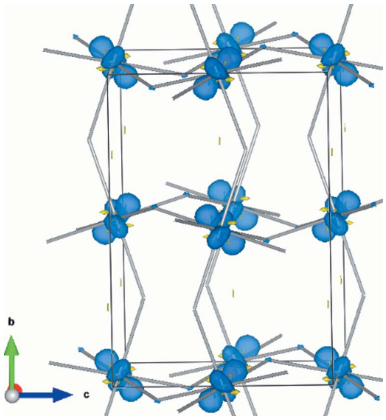

Figure 6
Spin density distribution. Isosurface is 0.40 e Å^{-2} (blue is positive, yellow is negative).

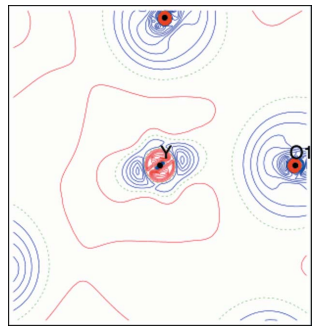

Figure 7
Static charge deformation density on the yttrium atom in the (010) plane. Contour level is 0.05 e Å^{-3}. Red contours are negative, blue contours are positive, dotted green is zero.

The model 3D spin density distribution in the unit cell is presented in Fig. 6. The contribution of the aspherical orbital ϕ_2 of titanium to spin density is clearly visible. The spherical contribution of orbital ϕ_1 is not visible in Fig. 6 as the maximal density localized on the center of titanium decreases quadratically with increasing distance from titanium. The presence of some regions with very weak negative spin distribution could be linked to artifacts in the experimental data.

Detailed information about population and orientation of atomic orbitals of the 'valence' shell for yttrium and oxygen atoms is given in Tables S7–S9. Fig. 7 presents the yttrium static charge deformation density in the (010) plane. The $|5s\rangle$ electrons are redistributed between the $|4d\rangle$ orbital of yttrium and the p orbital of O1 facing Y. This is also in agreement with the multipole model.

4. Conclusion

We have shown that the spin-resolved atomic orbital model is a reliable tool for analyzing charge and spin electron densities. It allows the characterization of the radial extension of atomic orbitals and directly provides their orientation and population. The atomic orbital and multipolar models are statistically equivalent to describe the electronic structure from experimental data.

When applied to the $YTiO_3$ perovskite, the atomic orbital model confirms the origin of the spin density which is mainly located on the titanium atom. It shows that not only t_{2g} orbitals are responsible for the magnetic moment but also the $|4s\rangle$ orbital of the titanium atom. The contribution of other orbitals to the magnetic moment is significantly weaker. For this mostly ionic crystal, the obtained net charges are close to the integrated charges over the Bader atomic basins.

Introducing 'bond' terms did not statistically improve the data refinement as $YTiO_3$ is mostly ionic. No significant spin contribution arising from the O1 atom was found, in contrast to the results obtained from the PND and XMD data analysis (Kibalin *et al.*, 2017). Further tests on more covalent materials like pyrite are on the way.

APPENDIX *A*
Modified Hamilton method

The Hamilton method was modified to apply linear and non-linear constraints during the least-squares refinement procedure. The constraints on the refined parameters, described in Section 2.4, can be written in a vector form with the equality

$$\mathbf{C}(\mathbf{p}) = \mathbf{0}, \tag{15}$$

where $\mathbf{p}$ is the vector of model parameters, $\mathbf{C}$ is the vector of constrained functions.

In the classical Hamilton method (Hamilton, 1964) the change of the model parameters $\Delta\mathbf{p}_{\rm new}$, which satisfies the linear constraints, is calculated as

$$\Delta\mathbf{p}_{\rm new} = \Delta\mathbf{p} - \Delta\mathbf{p}\cdot Q^{\rm T}\left(QH_{\mathbf{p}}^{-1}Q^{\rm T}\right)^{-1}QH_{\mathbf{p}}^{-1}, \tag{16}$$

where $H_{\mathbf{p}}$ is the Hessian over χ^2, $\Delta\mathbf{p}$ is the shift of model parameters without any restrictions on the refined parameters. The constraint matrix Q is estimated as

$$Q_{ij} = \left\{\left.\frac{\partial C_i}{\partial p_j}\right|_{\mathbf{p}_{\rm new}}\right\}. \tag{17}$$

For the linear type of constraints, the matrix Q is constant for any model parameter $\mathbf{p}$. Therefore, the derivatives calculated at the starting point $\mathbf{p}_0$ are equal to the derivatives calculated at the final point $\mathbf{p}_{\rm new}$. For a non-linear type of constraints, the solution of equation (16) taking into account (17) has to be found.

The solution can be established by applying an iterative procedure. The model parameters' shift calculated in the previous iteration $\Delta\mathbf{p}_n$ is used for estimating the matrix Q_n with the subsequent calculation of the shift of the model parameters for the next iteration $\Delta\mathbf{p}_{n+1}$:

$$Q_n = \left\{\left.\frac{\partial C_i}{\partial p_j}\right|_{\mathbf{p}_n}\right\}, \tag{18}$$

$$\Delta\mathbf{p}_{n+1} = \Delta\mathbf{p}_n - \Delta\mathbf{p}_n Q_n^{\rm T}\left(Q_n H_{\mathbf{p}}^{-1}Q_n^{\rm T}\right)^{-1}Q_n H_{\mathbf{p}}^{-1}, \tag{19}$$

$$\mathbf{p}_{n+1} = \mathbf{p}_n + \Delta\mathbf{p}_{n+1}. \tag{20}$$

This procedure works well with linear and non-linear types of constraints. It has been introduced into the *MOLLYNX* program (Deutsch *et al.*, 2012) to perform the least-squares refinement procedure under constraint conditions.

Funding information

We thank the ANR (Agence Nationale de la Recherche) through the MTMED project: multi-techniques modelling of electron densities. IK thanks the ANR for his postdoctoral position. ABV thanks the ANR for financial support.

References

Akimitsu, J., Ichikawa, H., Eguchi, N., Miyano, T., Nishi, M. & Kakurai, K. (2001). *J. Phys. Soc. Jpn*, **70**, 3475–3478.
Avery, J. & Watson, K. J. (1977). *Acta Cryst.* A**33**, 679–680.
Bader, R. F. W. (1990). *Atoms in Molecules – A Quantum Theory*. Oxford University Press.
Bentley, J. & Stewart, R. F. (1973). *J. Comput. Phys.* **11**, 127–145.
Bonham, R. (1965). *J. Phys. Soc. Jpn*, **20**, 2260–2262.
Brown, P. J., Capiomont, A., Gillon, B. & Schweizer, J. (1979). *J. Magn. Magn. Mater.* **14**, 289–294.
Bytheway, I., Figgis, B. N. & Sobolev, A. N. (2001). *J. Chem. Soc. Dalton Trans.* pp. 3285–3294.
Chandler, G. S. & Spackman, M. A. (1978). *Acta Cryst.* A**34**, 341–343.
Clementi, E. & Roetti, C. (1974). *At. Data Nucl. Data Tables*, **14**, 177–478.
Deutsch, M., Claiser, N., Pillet, S., Chumakov, Y., Becker, P., Gillet, J.-M., Gillon, B., Lecomte, C. & Souhassou, M. (2012). *Acta Cryst.* A**68**, 675–686.
Deutsch, M., Gillon, B., Claiser, N., Gillet, J.-M., Lecomte, C. & Souhassou, M. (2014). *IUCrJ*, **1**, 194–199.
Gillon, B. & Becker, P. (2011). In *Modern Charge-Density Analysis*, edited by C. Gatti & P. Macchi. Dordrecht: Springer.
Hamilton, W. C. (1964). *Statistical Methods in the Physical Sciences*. New York: Ronald Press.
Hansen, N. K. & Coppens, P. (1978). *Acta Cryst.* A**34**, 909–921.
Hester, J. R., Tomimoto, K., Noma, H., Okamura, F. P. & Akimitsu, J. (1997). *Acta Cryst.* B**53**, 739–744.
Holladay, A., Leung, P. & Coppens, P. (1983). *Acta Cryst.* A**39**, 377–387.
Iga, F., Tsubota, M., Sawada, M., Huang, H. B., Kura, S., Takemura, M., Yaji, K., Nagira, M., Kimura, A., Jo, T., Takabatake, T., Namatame, H. & Taniguchi, M. (2004). *Phys. Rev. Lett.* **93**, 257207.
Ito, M., Tuji, N., Itoh, F., Adachi, H., Arakawa, E., Namikawa, K., Nakao, H., Murakami, Y., Taguchi, Y. & Tokura, Y. (2004). *J. Phys. Chem. Solids*, **65**, 1993–1997.
Itoh, M. & Tsuchiya, M. (2001). *J. Magn. Magn. Mater.* **226–230**, 874–875.
Jelsch, C., Guillot, B., Lagoutte, A. & Lecomte, C. (2005). *J. Appl. Cryst.* **38**, 38–54.
Kibalin, I. A., Yan, Z., Voufack, A. B., Gueddida, S., Gillon, B., Gukasov, A., Porcher, F., Bataille, A. M., Morini, F., Claiser, N., Souhassou, M., Lecomte, C., Gillet, J.-M., Ito, M., Suzuki, K., Sakurai, H., Sakurai, Y., Hoffmann, C. M. & Wang, X. P. (2017). *Phys. Rev. B*, **96**, 054426.
Li, B., Louca, D., Hu, B., Niedziela, J. L., Zhou, J. & Goodenough, J. B. (2014). *J. Phys. Soc. Jpn*, **83**, 084601.
Mochizuki, M. & Imada, M. (2004). *New J. Phys.* **6**, 154.
Nakao, H., Wakabayashi, Y., Kiyama, T., Murakami, Y., Zimmermann, M. v., Hill, J. P., Gibbs, D., Ishihara, S., Taguchi, Y. & Tokura, Y. (2002). *Phys. Rev. B*, **66**, 184419.
Niehaus, T. A., López, R. & Rico, J. F. (2008). *J. Phys. A: Math. Theor.* **41**, 485205.
Raymond, K. N. (1972). *Acta Cryst.* A**28**, 163–166.
Schuchardt, K. L., Didier, B. T., Elsethagen, T., Sun, L., Gurumoorthi, V., Chase, J., Li, J. & Windus, T. L. (2007). *J. Chem. Inf. Model.* **47**, 1045–1052.
Schweizer, J. & Ressouche, E. (2001). *Magnetism – From Molecules to Materials*, edited by J. S. Miller & M. Drillon, pp. 325–355. Weinheim: Wiley-VCH.
Shmueli, U. (2001). Editor. *International Tables for Crystallography*, Vol. B, *Reciprocal Space*. Dordrecht: Kluwer.
Stevens, E. D. (1980). *Electron and Magnetization Densities in Molecules and Crystals*, edited by P. Becker, pp. 823–826. New York: Plenum Press.
Stewart, R. F. (1969). *J. Chem. Phys.* **51**, 4569–4577.
Stewart, R. F., Davidson, E. R. & Simpson, W. T. (1965). *J. Chem. Phys.* **42**, 3175–3187.
Tanaka, K. (1988). *Acta Cryst.* A**44**, 1002–1008.

Tanaka, K., Makita, R., Funahashi, S., Komori, T. & Zaw Win (2008). *Acta Cryst.* A**64**, 437–449.
Tsuji, N., Ito, M., Sakurai, H., Suzuki, K., Tanaka, K., Kitani, K., Adachi, H., Kawata, H., Koizumi, A., Nakao, H., Murakami, Y., Taguchi, Y. & Tokura, Y. (2008). *J. Phys. Soc. Jpn*, **77**, 023705.
Ulrich, C., Khaliullin, G., Okamoto, S., Reehuis, M., Ivanov, A., He, H., Taguchi, Y., Tokura, Y. & Keimer, B. (2002). *Phys. Rev. Lett.* **89**, 167202.
Voufack, A. B., Claiser, N., Lecomte, C., Pillet, S., Pontillon, Y., Gillon, B., Yan, Z., Gillet, J.-M., Marazzi, M., Genoni, A. & Souhassou, M. (2017). *Acta Cryst.* B**73**, 544–549.
Voufack, A. B., Kibalin, I., Yan, Z., Claiser, N., Gueddida, S., Gillon, B., Porcher, F., Gukasov, A., Sugimoto, K., Lecomte, C., Dahaoui, S., Gillet, J.-M. & Souhassou, M. (2019). *IUCrJ*, **6**, 884–894.
Vuković, T. & Dmitrović, S. (2010). *J. Phys. A: Math. Theor.* **43**, 455208.